Macromolecules
ARTICLE

Macromolecules **2010**, *43*, 4105–4112 **4105**
DOI: 10.1021/ma100328e

Phototriggered Mass Migrating Motions in Liquid Crystalline Azobenzene Polymer Films with Systematically Varied Thermal Properties

Jun Isayama, Shusaku Nagano, and Takahiro Seki*

Department of Molecular Design and Engineering, Graduate School of Engineering, Nagoya University, Furo-cho, Chikusa, Nagoya 464-8603, Japan

Received February 9, 2010; Revised Manuscript Received April 6, 2010

ABSTRACT: A family of homopolymers and random copolymers consisting of an azobenzene (Az)-containing methacrylate and hexyl acrylate were synthesized varying the copolymerization ratio. With increasing the content of hexyl acrylate, the temperature range of the liquid crystalline (LC) state was monotonously lowered. These polymer films were subjected to an exposure to the patterned irradiation to evaluate the mass transport behavior. This approach revealed that the efficient mass migration is strongly coupled with the thermal properties. Under the optimized conditions, two types of irradiation procedures were adopted: (i) two-step irradiation involving the UV (365 nm) light illumination and subsequent patterned visible light (488 nm of argon ion laser or 436 nm Hg line) and (ii) one-step patterned irradiation with UV light. After the irradiation with a photomak, the former method caused the mass transfer from the illuminated regions to shaded ones, whereas the latter led to the migration in the inversed direction. In both procedures, the migration consistently proceeded at the boundaries from the smectic A phase regions to the isotropic ones in the photochemically generated phase patterns. More general guidelines are proposed to exert the efficient mass transport in the LC Az polymers by adjusting the polymer design and temperature.

Introduction

Since the discovery in 1995,[1,2] the phenomenon of photoinduced mass migration in azobenzene (Az)-containing organic polymer films, leading to the surface relief formation, has been attracting great attention of materials chemists and physicists. This phenomenon is dubbed as photoinduced surface relief gratings (SRG) or photoinduced surface relief (PSR).[3−5] In this process, the trans−cis photoisomerization taking place at a molecule level is transformed to large-scale motions that reach distances of some micrometers. At the early stage of research, the systems are mostly limited to amorphous Az-containing polymer films;[1−5] however, recent activities have been rapidly accumulating new knowledge, expanding to other types of materials including amorphous low-molecular-mass compounds[6,7] and the surface of molecular crystals.[8] In view of chemical design of materials, many new attempts have recently been made. SRG systems based on the supramolecular basis (noncovalent attachment of the Az unit in the polymer design) are demonstrated,[9,10] and the photochromic units other than Az, such as spiropyran,[11] spyrooxazine,[12] diarylethene,[13] and hexaarylbiimidazole,[14] have also become fascinating targets in recent years. Not only pure organic systems but also organic−inorganic sol−gel processes have also been applied for the mass transfer of the films.[15−18]

Our work has been focusing onto liquid crystalline (LC) Az-polymer materials for SRG formation.[19−25] The mass migration is completed at uncommonly small dose levels (< 100 mJ cm^{-2}), which is 3 orders of magnitude smaller than those required for conventional amorphous polymer films.[19,20] Here the Az unit providing a long lifetime of cis-isomer is employed, and thus the photoirradiation with UV (365 nm) light leads to the smectic LC to isotropic phase transition.[22] The mass transport in the LC polymers occurs at boundary areas between the smectic LC and isotropic phases. Probably, the disparity in the viscosity and surface tension at the boundaries will promote the mass transfer. Besides the high sensitivity, the mass migration in the LC polymers has characteristic features such as (i) the process is insensitive to the light polarization,[23] (ii) the motion continues even after stopping the irradiation,[24] and (iii) the motion is initiated even by the sensitization from a dye absorbing longer wavelength.[22] All these facts support the interpretation that the driving mechanism in the LC polymer systems is fully different from that of the amorphous ones.[25] The process involved in the LC materials can be recognized as "phase transition type". The migration occurs basically as the thermal process via self-assembly of the polymer material, and the electromagnetic effect (gradient force) frequently considered for the amorphous systems[1−5] is, if any, negligible.

Our initial approach required particular polymer designs, namely, Az LC polymers embedding low-molecular-mass liquid crystal[19] and random copolymers containing a flexible oligo(ethylene oxide) side chain.[20,21] Without such additional components, the mass migration hardly occurs, which could be a drawback in expanded applications. As readily expected, the migration motions should be related to the thermophysical state of the polymer. In this context, we attempted to synthesize a family of polymers whose thermal properties are systematically tuned. Here, random copolymers was obtained from two components of an Az-containing methacrylate and hexyl acrylate varying the copolymerization ratio (Figure 1, pAz(x), x = 1.0, 0.96, 0.60, 0.38, 0.29, and 0.07, where x corresponds to the unit content of Az), and these polymers were subjected to the mass transport experiments. Since the glass transition temperature of poly(hexyl acrylate) is −57 °C,[26] the increased content of hexyl acrylate is expected to lower the phase transition temperatures. Another reason for the choice of hexyl acrylate is that this unit contains a simple hydrocarbon chain without polar or reactive

*To whom correspondence should be addressed. E-mail: tseki@apchem.nagoya-u.ac.jp.

Published on Web 04/15/2010

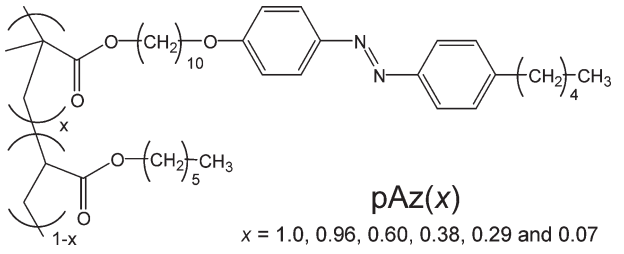

Figure 1. Chemical structure of a family of pAz(x) homo- and copolymers.

Table 1. Homo- and Copolymers of pAz(x) and Their Characterizations

	Az[a]:hexyl[b]					
polymer	feed	obtained	yield/%	$M_n/\times10^4$	M_w/M_n	layer spacing[c]/nm
pAz(1.0)	10:0	1.0:0	51	3.0	2.2	3.27[e]
pAz(0.96)	9:1	0.96:0.04	71	1.7	1.8	3.22
pAz(0.60)	5:5	0.60:0.40	58	1.6	1.6	4.37
pAz(0.38)	6:4	0.38:0.62	56	1.4	1.6	4.12
pAz(0.29)	4:6	0.29:0.71	61	1.6	1.6	f
pAz(0.07)	1:9	0.07:0.93	c	3.1	3.0	f

[a] Az-containing monomer. [b] Hexyl acrylate. [c] Room temperature. [d] Difficult to evaluate precisely due to viscous liquid nature of the polymer. [e] Taken from ref 29. [f] No diffraction peak.

functional group(s). This "inert" unit should avoid secondary complex effects such as strong molecular interactions and nanosegregations. Based on the knowledge obtained in this approach, more general view and versatility for the design and optimizations in the mass transfer systems via the photoinduced phase transition are obtained, which should be of great significance in further practical applications.

Experimental Section

Materials. 4-Pentylaniline, phenol, and α,α′-azobis(isobutyronitrile) (AIBN) were purchased from Kanto Kagaku Co. Ltd. 10-Bromo-1-decanol, methacryl chloride, and hexyl acrylate were obtained from Tokyo Chemical Industries Co. Ltd. Synthesis of 4-(10-methacryloyloxydecyloxy)-4′-pentylazobenzene (5Az10Me) monomer was described previously.[27]

Polymerization. A typical polymerization procedure is described as follows for the 50:50 molar feed ratio. 5Az10MA (0.5 g, 1.0 mmol), hexyl methacrylate (0.16 g, 1.0 mmol), and AIBM (6.6 mg, 1.0 wt % of the total monomer) were dissolved in dry tetrahydrofuran (THF, 5 mL) in an ample under a nitrogen atmosphere. This mixture was degassed by freeze−pump−thaw cycles three times. The ample was then sealed and heated at 80 °C while shaking in the dark for 20 h. The obtained polymer was purified by precipitation from THF to hexane three times to obtain a yellow powder.

The family of homopolymer and copolymers were synthesized in the same manners. The molar feed ratio of [5Az10Me]:[hexyl acrylate] was changed from 100:0 to 10:90 as listed in Table 1. The resulting copolymerization rations are also summarized in this table.

Methods. Fused silica plates used as substrates were cut in 10 × 15 mm size, cleaned by soaking in potassium oxide/ethanol solution for 30 min under sonication, washed by immersing in deionized water for 15 min twice, and finally dried by blowing nitrogen gas.

The polymer was dissolved in chloroform (1 wt %) and passed through a Millipore membrane filter (pore size: 0.2 μm). This solution was subjected to a spincast procedure at 2000 rpm for 30 s using a spin-coater Kyowariken K-359 S-1. The film was then heated at 80 °C for 3 min to remove solvents and anneal the film. The film thickness was ca. 50 nm as revealed by AFM measurement after scratching the film by a spatula.

Holographic recording was achieved by a single beam mode (Lloyd arrangement) where half of the beam was reflected by a mirror (M) set at a given angle. The intensity of recording beam from an argon ion (Ar^+) laser (Omnichrom 543R-AP-A01) after passing through the collimating lens (CL) was 2 mW cm^{-2}. The angle between the two writing beams was 7°, providing a grating periodicity of 4 μm. The (p-,p-) mode interference was adopted. As previously shown,[23] the difference in the polarization mode, i.e., (p-,p-) or (s-,s-), does not essentially influence the transport behavior in our systems. The formation process of SRG was monitored by the change in the first-order diffraction intensity of a helium−neon (He−Ne) laser beam on the transmission side using a photodetector.

Light irradiation (preirradiation with UV light and photopatterning with a photomask) was performed with a Hg−Xe lamp (UV Supercure-203, San-ei Electronic) passing through an appropriate optical filters (the combination of UV55 and UVD 35 (Toshiba) and Y-44 and V44 (Toshiba) for 365 and 436 nm line, respectively).

Measurements. Gel permeation chromatography was performed with a Shodex system (column: KF 803 and 805 L) combined with a UV detector (UV-41) using THF as the eluent. The molecular weight was calibrated by polystyrene standard.

^{1}H NMR spectra were taken in $CDCl_3$ on a JEOL JNM-GSX270. The copolymerization ratio was evaluated by comparing the integrated proton numbers of aromatic (Az) parts with respect to the ester (−O−CH_2−).

Differential scanning calorimetric (DSC) measurements were undertaken using a SSC5100 (SII). The scanning rate was 2 °C min^{-1} on the both heating and cooling process ranging from −80 to 150 °C.

The texture of liquid crystal was observed with an Olympus BH-2 polarizing optical microscope (POM) equipped with a temperature controlling stage (Mettler FP-80). The images were taken with a DP70 camera (Olympus).

X-ray diffraction (XRD) measurements were achieved with a Rigaku AX-G using a Cu Kα (0.154 nm) beam. The film sample was placed on a fused silica plate, and the scattered beams were observed on an imaging plate. (The temperature was changed using a Mettler FP-80 stage.)

For ordinary measurements of UV−vis absorption spectra, a Hewlett-Packard 8452A diode array spectrometer was used. To obtain spectra at elevated temperatures under illumination, homemade arrangements were achieved in the instrumentation (see Results and Discussion). The light source and detector employed were a DH-2000-BAL (Mikropack Inc.) and QE65000 (Ocean Optics Inc.), respectively. The probing light was guided via optical fibers. Light irradiation for the photoisomerization was performed from the side at an angle of 45° from the horizontal plane; therefore, the light intensity was corrected accordingly. Light intensity was evaluated using an Advantest optical power meter TQ8210. For light irradiation and measurements at elevated temperature, a PMC-730 (AS ONE) temperature-controlling plate was used.

Topographical surface morphologies were observed by atomic force microscopy (AFM) with a SII Nanopics 2100 in the dynamic force mode (Cantilever NPX1CTP004).

Results and Discussion

Polymer Synthesis and Characterizaions. *Synthesis.* The characterizations of the pAz(x) obtained by changing the monomer ratio are summarized in Table 1. The resulting copolymerization ratios (x) were estimated by ^{1}H NMR spectroscopy. The number-averaged molecular weight (M_n) and the polydispersity (M_w/M_n) evaluated by GPC, and the smectic layer spacing evaluated by XRD for film samples are also shown in this table. As shown, the resulting

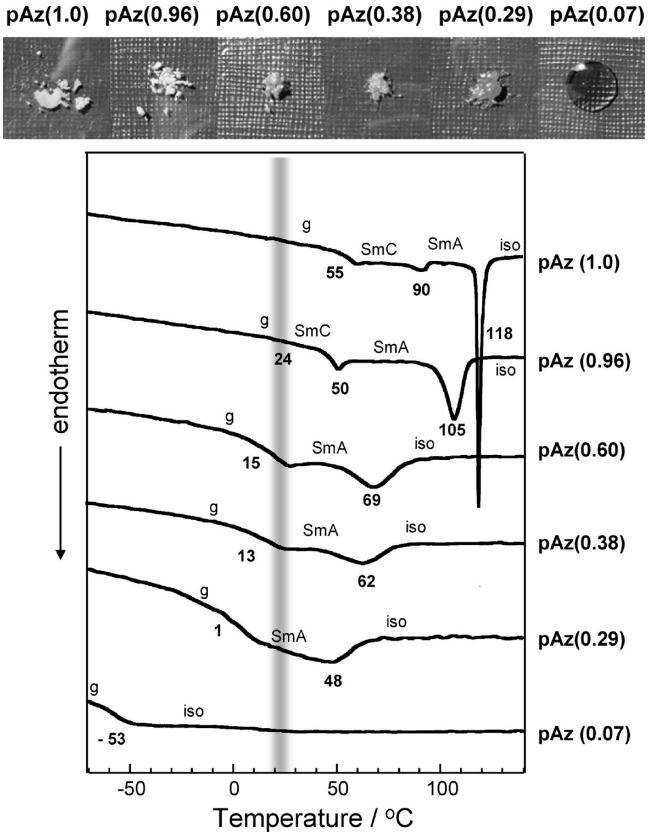

Figure 2. DSC profiles on the heating process for the family of pAz(x) homo- and copolymers. The photographs of the upper part display the appearance of polymer samples at room temperature. In the DSC chart, the identified phases are indicated (iso: isotropic; SmA: smectic A; SmC: smectic C; and g: glass state), and the hatched region corresponds to room temperature (20−23 °C).

copolymerization ratios approximately coincide with the feeding ratios. The number-averaged molecular weight ranged $(1.4-3.1) \times 10^4$.

Thermal Properties. In the upper part of Figure 2, the photographs of the polymers taken on a commercial digital camera are displayed to show the appearance of the polymer samples at room temperature. Polymers of the higher Az contents ($x = 1.0$ and 0.96) were obtained as fully dry yellow powders. As decreasing the Az content, the surface of powders looked slightly wet in appearance ($x = 0.60$, 0.38) and became sticky for $x = 0.29$. In the extreme case of $x = 0.07$, the polymer was obtained as viscous liquid. Thus, by simply observing the sample with naked eyes, one can recognize that the content of hexyl acrylate monotonously modifies the thermophysical state of the polymer.

In Figure 2, DSC profiles taken on the heating process for the six polymers are indicated. In the profiles, the identified phases by POM are also indicated. For the homopolymer (pAz(1.0)), T_g was observed at 55 °C. Small and large endothermic peaks were observed at 90 and 118 °C, respectively. The polymer adopted the isotropic state above 118 °C as revealed by POM observation. On the cooling process, growth of bátonnets in the isotropic melt[28] was admitted, indicating that the smectic A phase appears at 90−118 °C. At 55−90 °C, a broken fan-shaped texture, which is a characteristic one for the smectic C phase, was observed in POM. Below 55 °C, the texture was frozen to show the glassy state.

The effect of copolymerization with hexyl acrylate was obvious even at a small content (4 mol %) as shown for pAz(0.96). The transition to the isotropic phase became broadened and lowered to 105 °C and the transition from the smectic C to smectic A, and T_g was shifted to 50 and 24 °C, respectively.

The copolymerization with more amount of hexyl acrylate continuously shifted the transition temperatures to the lower regions. Below $x = 0.60$, the smectic C phase was not admitted. For pAz(0.07), T_g was observed at −53 °C, which almost agrees with a literature value for the homopolymer of poly(hexyl acrylate),[26] and no observable peak was admitted at higher temperatures.

The film thickness used in this work was ca. 50 nm. The thin state of the film may lead to some deviations in the thermal properties from those estimated by DSC for bulk polymer materials. In this respect, the thermal phase changes of thin films were monitored by UV−vis spectroscopic measurements. According to the spectroscopic data, the phase transition temperatures well agreed with those obtained by the DSC measurements. Furthermore, the thickness changes ranging from 50 to 200 nm did not alter the behavior. It is thus assumed that the thermophysical properties obtained by DSC are essentially retained in the thin films of 50 nm level.

XRD Measurements. The layer spacings of the smectic phase at room temperature are listed in Table 1. The data can be classified into three groups. The polymers providing the layer spacing of 3.2−3.3 nm (pAz(1.0) and pAz(0.96)), that of 4.1−4.4 nm, and no clear diffraction peak (pAz(0.29) and pAz(0.07)). Together with the POM data, the layer spacing for the first group reflects the frozen structure of smectic C phase. In comparison with the molecular length of the Az side moiety, the tilt angle can be estimated to be 45°. The second group gave the larger layer spacing, which probably reflects the smectic A without the molecular tilt. The clear diffraction peak was not observed for pAz(0.29); however, some highly disordered layer structures should be involved because the POM provided the birefringent character of smectic A phase. In the case of pAz(0.07), no regular structure was formed judging from a dark field image of POM observation.

Photoirradiation and Mass Transport Behavior. *Initial State before Irradiation*. At the initial state of the films before irradiation, the aggregation state of Az and its orientation with respect to the substrate plane depended on the Az content. The H-aggregates were partially formed in the films for the polymers with the higher Az contents. The absorption maximum of the $\pi-\pi^*$ band exhibited hypsochromic shift to 320 and 325 nm for pAz(1.0) and pAz(0.96), respectively. For the other films, the peak was positioned around 350−352 nm, indicating the absence of H-aggregation. The relative absorption intensity ratio of the $\pi-\pi^*$ band of Az (320−352 nm) to that of $\pi-\pi^*$ band of phenyl ring (ca. 250 nm) in the transmission spectra can be a rough indicator to estimate the orientation of trans-Az with the substrate plane. According to this estimation, the Az mesogenic units orient highly perpendicular to the substrate plane for pAz(1.0), pAz(0.96), pAz(0.60), and pAz(0.38). In the case of pAz(0.29), the orientation became more randomized, and pAz(0.07) adopted a fully randomized orientational state.

Such differences in the aggregation and molecular orientation may affect the migration behavior as will be described below; however, we infer that the initial aggregation state and orientational order of Az are of less importance judging from the following fact. The irradiation with 365 nm light quickly destroys the Az aggregation at an early stage of low cis-Az content. The migration is essentially initiated from the nonaggregated and orientationally randomized state.

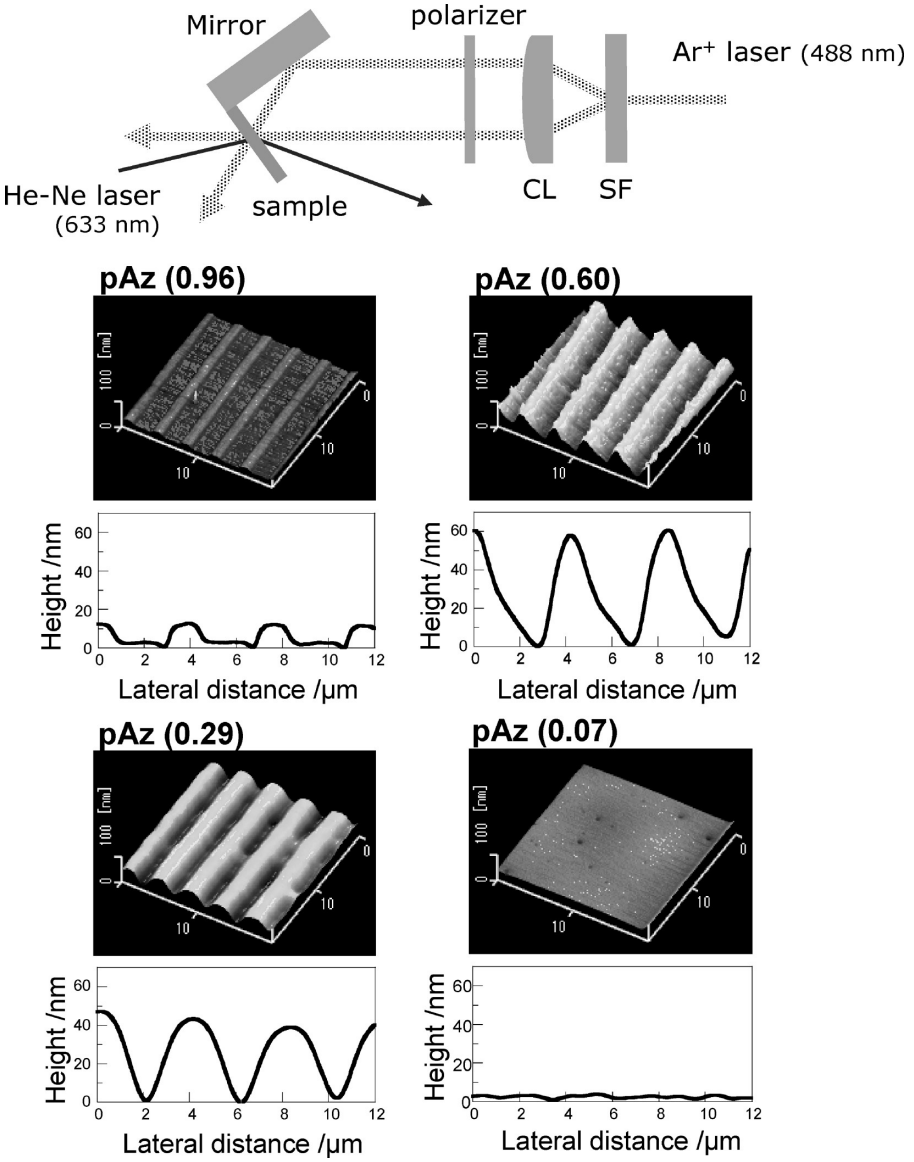

Figure 3. SRG formation by irradiation with interference argon ion laser beam. Topographical AFM images and height profiles are shown. Four polymer films with different thermophysical properties, pAz(0.96), pAz(0.60), pAz(0.29), and pAz(0.07), were employed. In the upper part, the experimental setup (Lloyd-type interference arrangement) is depicted. CL and SF indicate collimating lens and scattering filter, respectively.

For the thin films employed for the SRG formation (ca. 50 nm thickness), the birefringent character was not admitted in the polarized optical microscopic observation. However, it is naturally assumed that similar domain structures are formed even in the thin films as are observed for thicker ones (see POM images in Figure 8 shown later).

Interference Laser Beam Irradiation at Room Temperature. Figure 3 indicates the inscribed SRG structures observed by AFM for the films of pAz(0.96), pAz(0.60), pAz(0.29), and pAz(0.07). In these experiments, a Lloyd-type interference setup was constructed as displayed in the upper scheme of Figure 3. The films were preirradiated with 365 nm light to the photostationary (cis-rich) state, and subsequently the interference argon ion laser beam (488 nm, 2.0 mW cm^{-2}) was irradiated. As clearly shown, the modulation depth (depth from the top to valley) strongly depended on the Az content. Large modulation depths were obtained for pAz(0.60) and pAz(0.29). The modulation depth significantly reduced for pAz(0.96), and virtually no relief formation was observed for pAz(1.0) (data not shown). Also in the case of pAz(0.07), no surface relief structure was recognized. The asymmetric shape particularly seen for pAz(0.60) film in the relief structure was not reproducible and can be regarded as an artifact. The shape asymmetry could be caused by subtle experimental setup conditions.

Since the trans-to-cis photoisomerization underwent sufficiently at the photostationary state (cis content $>80\%$) for all polymer films, the difference in the transport behavior can be ascribed to the physical state of the trans-Az state. pAz(0.60) and pAz(0.29) show the smectic A phase at room temperature. The relief structure was efficiently formed for pAz(0.38) in the same manner (data not shown). In contrast, pAz(0.96) and pAz(0.07) are in the different physical state at room temperature; i.e., the former is in a frozen glassy state preserving the smectic C structure and the latter the isotropic (liquid) one. In Figure 3, the hatched area in the DSC chart displays the room temperature region. Therefore, it is assumed that the efficient transport at room temperature occurs when the trans-Az film is in the smectic A phase at this temperature.

By monitoring the first-order diffraction intensity of He−Ne laser beam, the transient and more quantitative

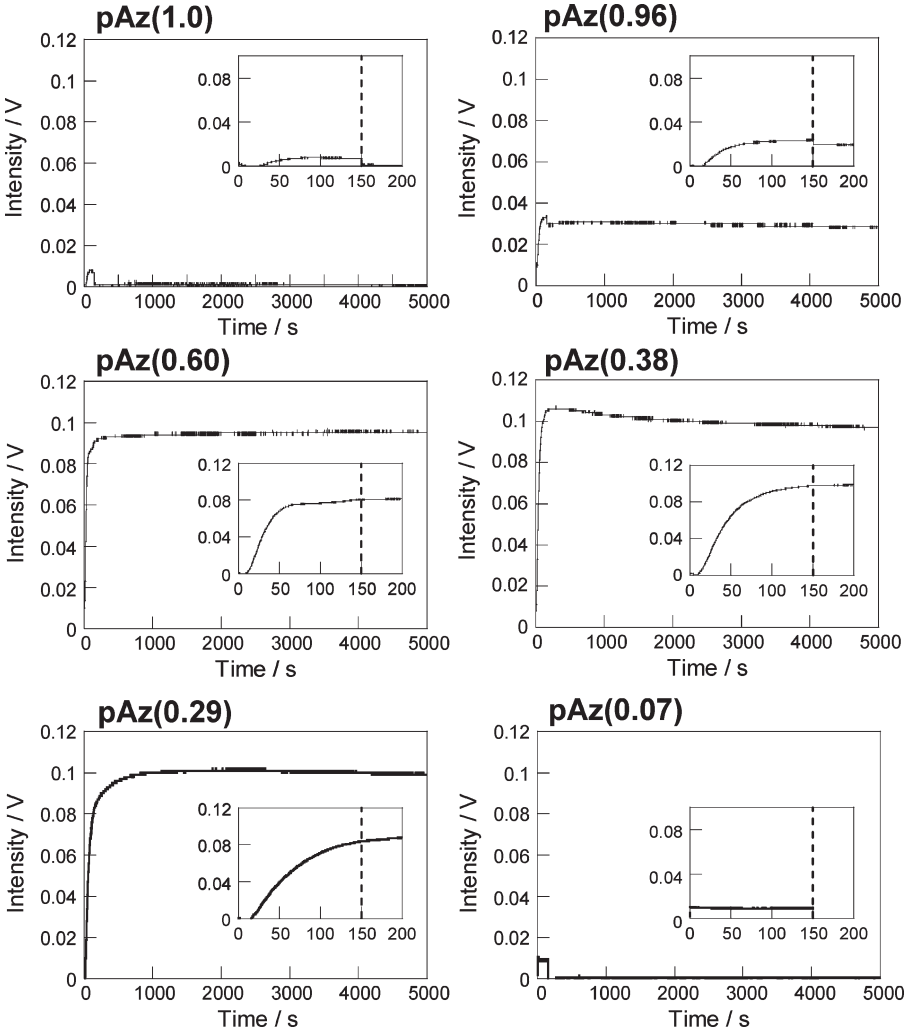

Figure 4. Time course profiles of the first-order diffraction of He−Ne laser beam to evaluate the SRG growth for all polymers. In the ordinate axis, the first-order diffraction intensity is expressed simply by the voltage of the detector. The irradiation with argon ion laser beam is stopped at 150 s. The insets indicate the magnified profiles at the initial stage.

evaluations could be available. Figure 4 shows the time course profiles under the exposure to the interference laser beam (2.0 mW cm^{-2}) at room temperature for the six polymers. The irradiation was intentionally stopped at 150 s. The inset in each figure depicts the magnified profiles at the initial stage. On the basis of the time-course profile features, the polymers are again classified into three groups. (i) pAz(1.0) and pAz(0.96): The rise in the diffraction intensity is negligible (x = 1.0) or insufficient (x = 0.96). The mass transfer was not effectively induced. For these two polymers, the smectic A phase appears at higher temperatures (> 50 °C) in the trans-Az state. The mass transfer occurred partially for pAz(0.96) since the segmental motion of the polymer chain is not fully frozen (T_g = 24 °C near the room temperature). (ii) pAz(0.60), pAz(0.38), and pAz(0.29): As also indicated in Figure 3, these polymers were most suited for SRG formation where efficient mass transfer takes place. These polymers adopt the smectic A phase at room temperature in the trans-Az state. The diffraction intensity is retained at high levels even after stopping the irradiation, indicating that the viscosity of the polymer in the trans-rich state of Az is sufficiently high to preserve the relief structure. (iii) pAz(0.07): The mass migration was negligible, and after stopping the irradiation, the small diffraction intensity immediately diminished (see the inset for pAz(0.07)).

Therefore, it is concluded from the AFM observations (Figure 3) and time-course diffraction profile data (Figure 4) that the efficient mass migration occurs for the polymer films when they adopt the smectic A phase in the trans-Az state at room temperature, namely the frequently adopted ambient experimental condition. This issue is in agreement with our former results that the previous Az LC polymer copolymerized with an oligo(ethylene oxide) unit shows the smectic A phase at 16−85 °C.[21]

The mass migration was mostly completed at 300 mJ cm^{-2} (2 mW cm^{-2}, 150 s). Further irradiation such as 2000 mJ cm^{-2} did not essentially changed the relief structure as far as the same intensity condition was employed.

Photomask Irradiation with Hg Lamp at Elevated Temperatures. According to the above aspect, the efficient mass migration may occur even for the pAz(1.0) and pAz(0.96) when the photoirradiation is performed at higher temperatures where the polymers adopt the smectic A phase. Therefore, our efforts were next shifted to the irradiation experiments using a photomask, which enables facile photopatterning procedures at controlled (higher) temperatures. Further, the photomask experiments have the advantage that the migrating direction can be easily recognized by a comparison with characteristic patterns of the mask.

Two methods were employed for the photopatterning, which are schematically illustrated as methods A and B in

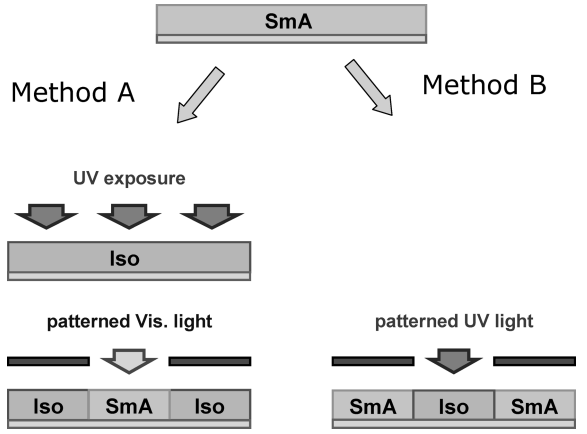

Figure 5. Schemes of the photopatterning procedures with a photomask. Method A: patterning with visible light after preirradiation with UV light. Method B: direct photopatterning with UV light.

Figure 5. Method A is basically the same procedure adopted for the laser beam experiment described previously.[19−24] The spin-cast film of pAz(x) was first irradiated with UV light over the whole area and then photopatterning with a photomask was achieved with visible line (436 nm) of Hg lamp. Method B involves only a single patterned irradiation with UV light (2 mW cm^{-2}) at a controlled elevated temperature. In both cases, the spatial micropatterns consisting of smectic A and isotropic phases will be formed on the Az polymer films.

The polymer of pAz(0.96) with higher T_g was employed for the photomask pattern experiments to verify the validity of the temperature control. The photomask possessed a figure "8" and line (10 μm)-and-space (15 μm) patterns. In Figure 6, the mask patterns (a), top view AFM topographical images of the surface relief morphology formed by method A at 80 °C (b), and method B at room temperature (c) and 80 °C (d) are depicted. At 80 °C this polymer shows the smectic A phase in the trans-Az state.

In method A at 80 °C, an efficient mass migration occurred as expected in a similar fashion as observed for p(0.60), p(0.38), and pAz(0.29) and the previous polymer systems at room temperature.[19−21] In method B, under the UV irradiation conditions employed, only slight relief formation was observed at room temperature (c), whereas an efficient and large mass transfer was observed at 80 °C (d), leading to the sufficient surface relief formation. These results strongly support the assumption drawn above that the mass migration efficiently takes place when the temperature condition is properly adjusted whatever the polymer material is. In other words, the special polymer design is not a requisite, but many types of LC Az polymers should be applicable when the pattern irradiation is performed at a proper temperatures where the polymer adopts the smectic A phase.

The polymer migration occurred from the irradiated regions to shaded ones in method A (see b), and in contrast, just the reversed motions were observed in method B (see d). To check the transport direction, the topological feature of two shaded rectangular spots in the center of figure "8" is of use. The film material in the two rectangles was up-lifted than the surroundings for method A (Figure 6b) and, in contrast, down-leveled in method B (Figure 6d). These apparently contrasting motions are consistently understood by the situation that the mass migration takes place at the boundary from the smectic A regions to isotoropic ones (see the phase state in Figure 5). Consequently, light can induce motions of both directions with respect to the photomask

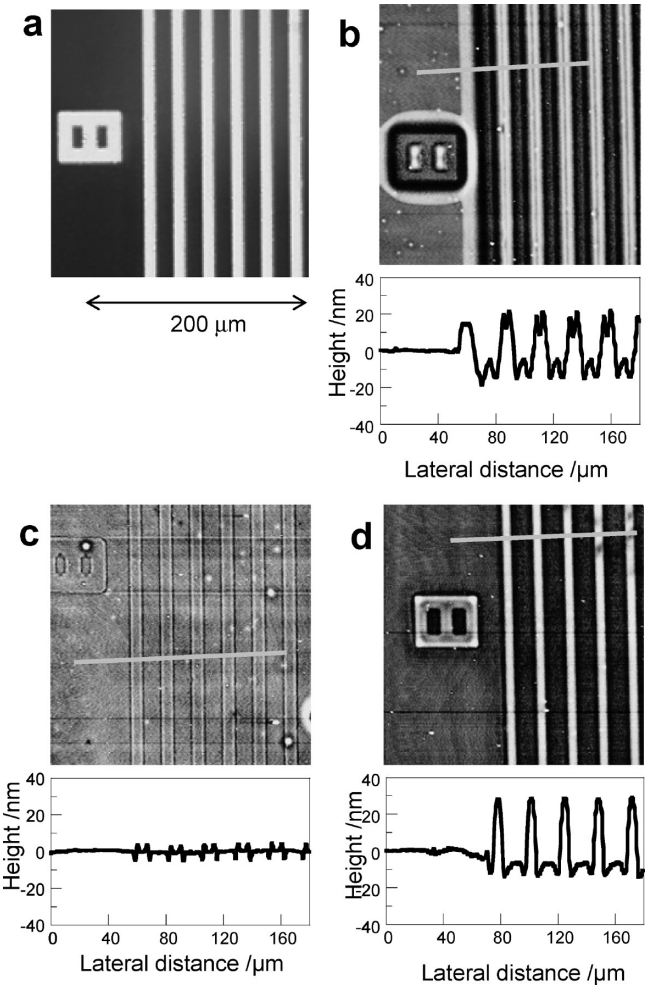

Figure 6. Top view topographical AFM images and height profiles along the line shown in the image for pAz(0.96) film after photoindicription by methods A and B. The pattern of photomask is shown in (a). AFM images of the pAz(0.96) film after photopatterning by method A at 80 °C (b), after photopatterning by method B at room temperature (c), and at 80 °C (d). The height profile of each figure was taken along the white line. Note that the surface concavo-convex features are reversed between the two methods with respect to the photomask pattern (compare (b) and (d)).

window by choosing the wavelength. It is to be noted that method B led to more precise relief morphologies with less distortions (compare b and d in Figure 6). This can be explained by the fact that the fluidization by UV irradiation occurs locally within a firm matrix of smectic A phase for method B. In method A, on the other hand, the local fixation occurs by visible light irradiation within a fluid matrix of isotropic phase, which should cause larger morphological deviations from the mask pattern shape.

Photoisomerization and Phase Transition Behavior at Higher Temperature. Our scenario on the mass migration is based on the photoinduced phase transition form the smectic A phase to isotropic one. It is of essence to confirm whether the trans-to-cis photoisomerization actually undergoes to sufficient levels at elevated temperatures for the induction of the phase transition to the isotropic phase. For this purpose, UV−vis spectroscopic and POM measurements were made at 80 °C.

Figure 7 depicts the modified instrumentation for UV−vis spectroscopic measurements in the heated conditions (upper) and spectral changes of pAz(0.96) film upon UV light illumination (365 nm, 0.28 mW cm^{-2}) at 80 °C (a) and

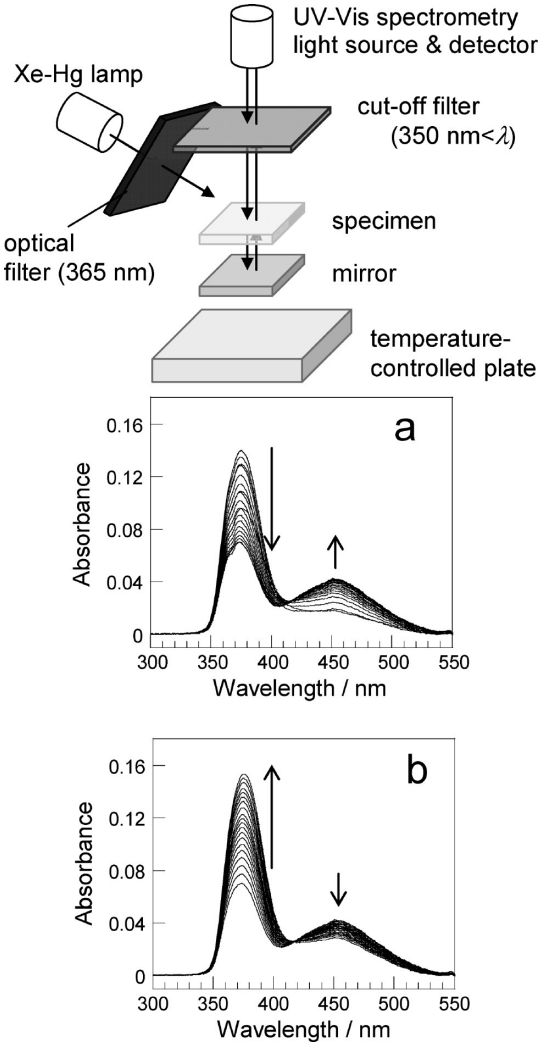

Figure 7. Schematic illustration of a setup for observation of UV−vis absorption spectral changes under illumination at elevated temperatures (upper) and absorption spectra under UV light illumination at 0.28 mW cm^{-2} for 0−200 s (a) and in the dark for 0−400 s after stopping UV illumination (b) at 80 °C.

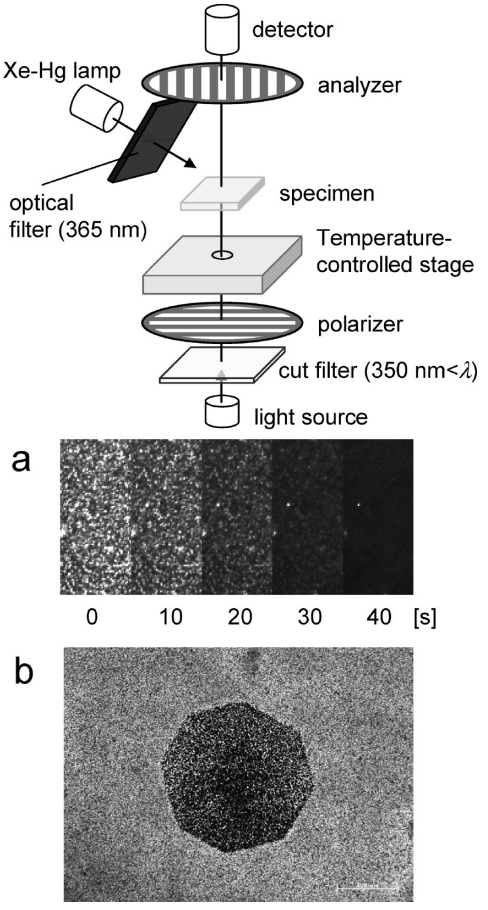

Figure 8. Schematic illustration of a setup for POM observation under illumination at elevated temperatures (upper). In the figures, changes in the POM image with time under UV light irradiation at 0.28 mW cm^{-2} for pAz(0.96) film (a) and image after spot UV illumination (diameter: 350 μm) of the same film at 80 °C are shown. The dark region corresponds to the photoinduced isotropic phase.

during the thermal back-reaction without irradiation at the same temperature (b). These spectral shapes do not express the actual ones because the wavelength region shorter than 350 nm was cut off by an optical filter. Nevertheless, these spectral changes provide sufficient information on the extent of photoisomerization. At the photostationary state of 365 nm irradiation at 0.28 mW cm^{-2}, the content of cis isomer reached ca. 50%. Since the accumulation of cis isomer is the competition with the thermal back-reaction, the cis content at the photostationary state depended on the light intensity. Irradiation at 1.0 mW cm^{-2} gave a cis content of 70−80%. (The UV light irradiation for the mass transfer in the previous section was performed at 2 mW cm^{-2}, and the cis content should be larger than this.) According to our previous study,[22] the smectic A to isotropic phase transition is brought about when the cis isomer is accumulated above ca. 40%. Thus, the spectral data suggest that the phase transition should be induced in these irradiation conditions. For the thermal back-reaction (b), the spectrum reverted to that of pure trans-Az isomer within 600 s.

The upper scheme of Figure 8 shows the scheme of setup for POM observations at elevated temperatures. As indicated in Figure 8a, the smectic A to isotropic phase transition was in fact induced at 80 °C upon UV light irradiation. At the initial state, the film of pAz(0.96) exhibited a sandlike texture composed of birefringent LC multidomains, a typical feature observed for side-chain polymer LC polymer. Upon UV light irradiation, the POM image became darker with time and eventually to a fully dark one after 40 s at 0.28 mW cm^{-2} (a). The dark image recovered to the initial texture while keeping at 80 °C. In (b), the POM image after spot irradiation (350 μm diameter) was shown. A distinct dark region appeared selectively at the irradiated spot due to the proceeding of the photoinduced phase transition. Of course, the UV irradiation with larger energy dose led to the faster phase transition. The data of rather small dose (0.28 mW cm^{-2}) was selected just for a comprehensive demonstration.

These spectroscopic and POM observations provide the clear evidence for the photoinduced phase transition of the pAz(0.96) film at the high temperature, and rationalize the occurrence of the efficient mass transport, as was observed for pAz(0.60), pAz(0.38), and pAz(0.29) in this study and those reported previously[20,21] at room temperature. It is assumed that, when the thermal back-reaction becomes too fast at higher temperatures, the induction of phase transition to the isotropic phase will be suppressed. In such cases, more intense UV light will be required.

Superimposed Inscription. In method A, superimposed inscription is unavailable in principle since the preirradiation with UV light fully erases the former relief structure due to

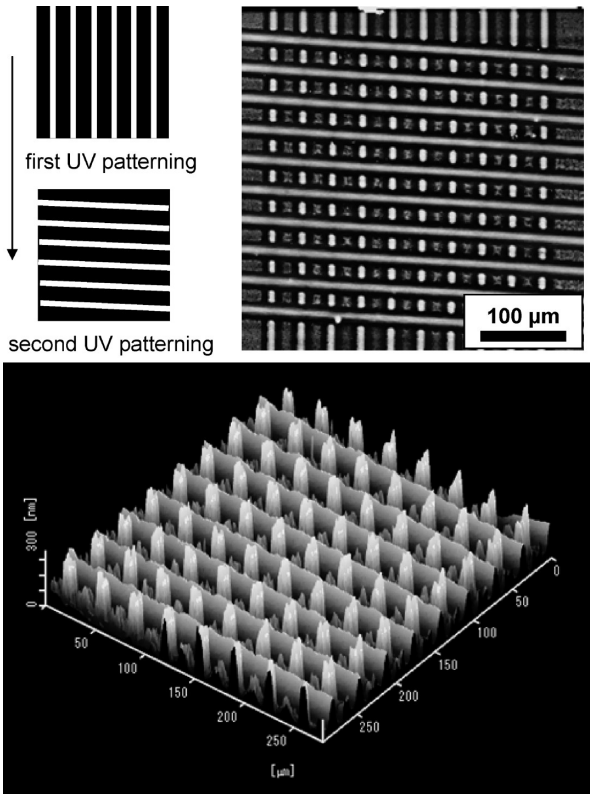

Figure 9. Resulting surface relief structure after superimposed inscription of pAz(0.60) film using a line (10 μm)-and-space (15 μm) photomask. Upper and lower images indicate the top view and bird's-eye view of the topographical AFM image. The mask pattern is displayed in the upper left, and the irradiation was performed as indicated.

the surface tension in the fluidized cis-rich isotropic state.[21] In contrast, the overwriting procedure should make sense in method B. Figure 9 indicates an example of superimposed inscription at room temperature using a pAz(0.60) film. The first inscription was made with a striped photomask in the vertical position of the figure. Subsequently, the second irradiation was performed with the stripe rotated at ca. 80° of the first irradiation. In this way, the overwriting procedure with UV irradiation was successfully achieved. In general, this type of overwriting process gives an emboss structure with uniform height in a cubic arrangement.[4,16] In contrast, the morphology feature of the relief obtained in this case is characterized by line stripes inscribed by the second irradiation and aligned dots existing between the lines which are the residuals of the first inscription. Thus, the morphology due to the first irradiation is fully rewritten at the local regions by the second inscription, which can be a particular feature observed in the highly mobile migration system of soft LC system.

Conclusions

The phototriggered mass migration behavior was examined using a series of random copolymers consisting of an LC Az side chain and a hexyl group with varied copolymerization ratios. This approach revealed the important roles of the thermophysical state of the polymer in the phototriggered mass migration. The efficient migration proceeds when the smectic A (trans-Az state) to isotropic phase (accumulated cis-Az content) transition properly occurs. The optimized conditions can be adjusted by both polymer design and temperature control. Since the polymer design and synthesis are rather tedious, the temperature control should be a more versatile strategy. In the photopatterning procedure with a photomask, the irradiated regions can be dents (likewise positive-type photoresists) or projections (negative-type) depending on the wavelength light irradiation. In addition to the rewritable nature, this discrimination can be one of the marked features of mass migrating systems, which is unavailable in development-based resist materials. When UV light is employed for the micropatterning, the superimposed inscription could be further feasible. The knowledge obtained in this work will largely extend the possibility of applicable materials in the exertion of phototriggered mass transfers systems based on the photoinduced phase transition. The materials choice is not be limited to organic polymer systems but can be extend to LC organic−inorganic hybrids.[17,18]

Acknowledgment. We thank Dr. N. Zettsu (mass transfer experiments) and M. Hara (X-ray measurements) for their technical assistance and helpful discussions. This work was supported by a Grant-In-Aid Scientific Research for Priority Areas "New Frontiers in Photochromism (No. 471)" of the Ministry of Education, Culture, Sports, Science and Technology, Japan.

References and Notes

(1) Rochon, P.; Batalla, E.; Natansohn, A. *Appl. Phys. Lett.* **1995**, *66*, 136–138.
(2) Kim, D. Y.; Tripathy, S. K.; Li, L.; Kumar, J. *Appl. Phys. Lett.* **1995**, *66*, 1166–1168.
(3) Natansohn, A.; Rochon, P. *Chem. Rev.* **2002**, *102*, 4139–4176.
(4) Viswanathan, N. K.; Kim, D. Y.; Bian, S.; Williams, J.; Liu, W.; Li, L.; Samuelson, L.; Kumar, J.; Tripathy, S. K. *J. Mater. Chem.* **1999**, *9*, 1941–1955.
(5) Yager, K. J.; Barrett, C. J. *Curr. Opin. Solid State Mater. Sci.* **2001**, *5*, 487–494.
(6) Nakano, H.; Takahashi, T.; Kadota, T.; Shirota, Y. *Adv. Mater.* **2002**, *14*, 1157–1160.
(7) Ishow, E.; Lebon, B.; He, Y.; Wang, X.; Bouteiller, L.; Galmeche, L.; Nakatani, K. *Chem. Mater.* **2006**, *18*, 1261–1267.
(8) Nakano, H. *J. Phys. Chem. C* **2008**, *112*, 16042–16045.
(9) Kulikovska, O.; Goldenberg, L. M.; Stumpe, J. *Chem. Mater.* **2007**, *19*, 3343–3348.
(10) Zettsu, N.; Ogasawara, T.; Mizoshita, N.; Nagano, S.; Seki, T. *Adv. Mater.* **2008**, *20*, 516–521.
(11) Ubukata, T.; Takahashi, K.; Yokoyama, Y. *J. Phys. Org. Chem.* **2007**, *20*, 981–984.
(12) Ubukata, T.; Fujii, S.; Yokoyama, Y. *J. Mater. Chem.* **2009**, *19*, 3373–3377.
(13) Ubukata, T.; Yamaguchi, S.; Yokoyama, Y. *Chem. Lett.* **2007**, *36*, 1224–1225.
(14) Kikuchi, A.; Harada, Y.; Yagi, M.; Ubukata, T.; Yokoyama, Y.; Abe, J. *Chem. Commun.* **2010**, *46*, 2262−2264.
(15) Darracq, B.; Chaput, F.; Lahlil, K.; Levy, Y.; Boilot, J. P. *Adv. Mater.* **1998**, *10*, 1133–1136.
(16) Kulikovska, O.; Goldenberg, L. M.; Kulikovsky, L.; Stumpe, J. *Chem. Mater.* **2008**, *20*, 3528–3534.
(17) Nishizawa, K.; Nagano, S.; Seki, T. *Chem. Mater.* **2009**, *21*, 2624–2631.
(18) Nishizawa, K.; Nagano, S.; Seki, T. *J. Mater. Chem.* **2009**, *19*, 7191–7194.
(19) Ubukata, T.; Seki, T.; Ichimura, K. *Adv. Mater.* **2000**, *12*, 1675–1678.
(20) Zettsu, N.; Ubukata, T.; Seki, T.; Ichimura, K. *Adv. Mater.* **2001**, *13*, 1693–1697.
(21) Zettsu, N.; Seki, T. *Macromolecules* **2004**, *37*, 8692–8698.
(22) Zettsu, N.; Ogasawara, T.; Arakawa, R.; Nagano, S.; Ubukata, T.; Seki, T. *Macromolecules* **2007**, *40*, 4607–4613.
(23) Zettsu, N.; Fukuda, T.; Matsuda, H.; Seki, T. *Appl. Phys. Lett.* **2003**, *83*, 4960–4962.
(24) Ubukata, T.; Hara, M.; Ichimura, K.; Seki, T. *Adv. Mater.* **2004**, *16*, 220–223.
(25) Seki, T. *Curr. Opin. Solid State Mater. Sci.* **2006**, *10*, 241–248.
(26) Rehberg, C. E.; Faucette, W. A.; Fisher, C. H. *J. Am. Chem. Soc.* **1944**, *66*, 1723–1724.
(27) Li, W.-H.; Nagano, S.; Seki, T. *New J. Chem.* **2009**, *33*, 1343–1348.
(28) Dirking, I. *Textures of Liquid Crystals*; Wiley-VCH: Weinheim, 2003; pp 91−93.
(29) Uekusa, T.; Nagano, S.; Seki, T. *Langmuir* **2007**, *23*, 4642–4645.